ELECTRONIC SUPPLEMENTARY INFORMATION

Role of Theory in the Design of Semiconducting Nanostructures

Vladan Mlinar*

Electronic Structure Calculations of Semiconducting Nanostructures

In the main body of the manuscript we discussed the direct, inverse, and synergistic predictive theory-experiment approaches used to link structure and property of semiconducting nanostructures. The underlying assumption behind all three approaches is that the employed theoretical model linking the structure and property, is sophisticated enough to handle nano systems of few thousands up to hundred of thousands of atoms including excitations and many-body effects. A model for electronic structure calculation should use as an input realistic geometry and composition profile, presumably extracted from structural characterization measurements, and take into account all of the relevant effects, including the strain and piezoelectric effects (if present),[1,2] and external magnetic[3–5] and electric fields.[6]

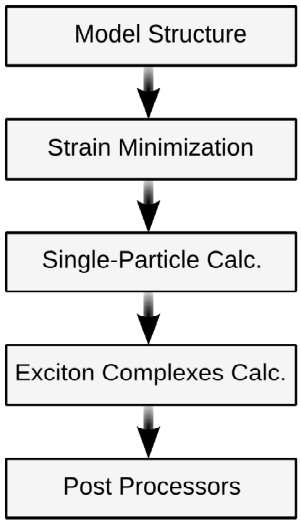

Fig. A Flowchart of the methodology used for electronic structure calculations of semiconductor nanostructures.

Ideally, the electronic structure of nanostructures should be calculated from the atomistic first-principles, e.g., Hartree Fock, Density Functional Theory, GW, but those methods are limited to systems with couple of hundreds of atoms. Modeling of nanostructures containing thousands up to hundred thousands or even several millions, requires empirical methods with input from experiment, e.g. effective masses, band gaps, deformation potentials. Several such empirical methods have been employed ranking from empirical atomistic, tight-binding[7,8] and pseudopotentials,[9–12] to continuum, envelope function,[3,4,13–18] models.

The flowchart of the methodology typically used for electronic structure calculations of semiconductor

*Research Institute for Advanced Materials Design, Boulder, Colorado 80302, USA. E-mail: vladan.mlinar@riamd.org;
School of Engineering, Brown University, Providence, RI 02912, USA; E-mail: vladan_mlinar@brown.edu; Tel: (+1)401-863-5231*

nanostructures is shown in Figure A. First, the model structure is defined, typically using available experimental data [Sec. 1]. Next, the strain distribution in and around such a model nanostructure is calculated [Sec. 2]. Then, the single particle states are calculated [Sec. 3]. The nature of many-particle interaction, including the electron-hole Coulomb effects, electron-hole exchange interaction, or correlations can be extracted from configuration-interaction calculations as explained in Sec. 4. Finally, the output of CI calculations is used in different post-processing tools, depending on the problem [Sec. 6 of ESI]. For example, this includes the calculation of the multiexcitonic emission spectra,[19–21] fine structure splittings of exciton complexes,[12,22] energy transfer for semiconductor nanocrystals,[23] charging energies, entanglement[6,24] to name just a few.

Methods for the electronic structure calculations of nanostructures were originally developed and applied to bulk materials. Thus, in what follows, we first review those methods as they were implemented for bulk and then discuss details of how a particular methodology was applied to nanostructures. We also address a gauge invariant implementation of magnetic field effects for nanostructures.

1 Model Structure

A model nanostructure is defined through its geometry and composition profile. Typically, the geometry and composition profile are extracted from structural characterization measurements. For the effective mass models, the structure is typically defined on a three-dimensional rectangular grid, where each and every node of the grid contains information about material forming nanostructure.[4,13,25,26] Potentials, effective masses, are constructed from this "structural grid". For atomistic models, initially the atoms are placed on a regular grid. For example, for $In_xGa_{1-x}As$ alloy, the N_{cat} cation sites are randomly populated by In or Ga atoms so that overall composition is x=X(In).[12]

If there is a lack of structural characterization data on the nanostructure, the geometry and composition profile are assumed, taking into account other available experimental data, such as photoluminescence (PL).For example, if there are available PL data, performed on an ensemble of semiconductor self-assembled quantum dots (QDs), the information about the individual properties, both structural and optical, of the QDs are lost, and model QD is actually as a representative of the ensemble of QDs.

2 Strain Minimization

If the nanostructure is strained, strain minimization of the model structure is performed next. Here we discuss the isotropic-elasticity (IE),[27] continuum elasticity (CE),[2,28] and valence force field (VFF) models.[29,30]

The strain distribution is calculated under the assumption that a nanostructure is already formed. The nanostructure made of one material is embedded in a surrounding material with different lattice constant. The elastic energy of such a system is minimized giving as a result the components of the strain tensor. It is clear that size, shape, composition profile as well as the growth on high index planes influence significantly the strain distribution.[31] Elastic constants that characterize the constituent materials forming the nanostructure, have values extracted from experiment, and enter the calculations regardless of the employed model.

Interestingly, the link with the experiment can be established at this step. Namely, it is possible to extract strain components from high resolution transmission electron microscopy (HRTEM) images of the sample,

enabling a comparison between calculated components of the strain tensor and strain components extracted from these HRTEM images.[32–35]

2.1 Isotropic Model:

Isotropy-elasticity (IE) model was proposed by Davies[27] and is based on the Eshelby's theory of inclusions[36]. It was shown that the elastic field may be derived from a scalar potential that obeys a Poisson equation with the lattice mismatch as charge density. The displacement was made analogous to the electric field providing a simple way to visualize the distortion around a nanostructure.

2.2 Continuum Elasticity:

In the continuum elasticity model,[2,28] the functional form of the elastic energy is minimized in order to obtain the distribution of the displacement in the structure, where from the strain is extracted.

The total elastic strain energy E_{CE} for a semiconductor material is given by:[2,28]

$$E_{CE} = \int \frac{1}{2} C_{ijkl}[e_{ij}(\mathbf{r}) - e^0_{ij}(\mathbf{r})][e_{kl}(\mathbf{r}) - e^0_{kl}(\mathbf{r})]dV \ , \tag{1}$$

where C_{ijkl} is the elastic modulus tensor, $e_{ij}(\mathbf{r})$ is the strain tensor, and $e^{(0)}_{ij}(\mathbf{r})$ is the local intrinsic strain induced by changes in the lattice constant; ijkl run over the coordinate system.

For a cubic system, assuming abrupt interfaces*between* a nanostructure and barrier material, that the coordinates are fixed to the barrier material, and treat the nanostructure as expanded barrier materials with different elastic constants, the total elastic energy is given

$$\begin{aligned} E_{CE} &= \int \frac{1}{2}[C_{11}(e^2_{xx}(\mathbf{r}) + e^2_{yy}(\mathbf{r}) + e^2_{zz}(\mathbf{r})) + C_{12}(e_{xx}(\mathbf{r})e_{yy}(\mathbf{r}) + e_{xx}(\mathbf{r})e_{zz}(\mathbf{r}) + e_{yy}(\mathbf{r})e_{zz}(\mathbf{r})) \\ &+ 2C_{44}(e^2_{xy}(\mathbf{r}) + e^2_{yz}(\mathbf{r}) + e^2_{xz}(\mathbf{r})) - 2\alpha e_0(e_{xx}(\mathbf{r}) + e_{yy}(\mathbf{r}) + e_{zz}(\mathbf{r})) + 3\alpha e^2_0]dV \ , \end{aligned} \tag{2}$$

Where

$$e_0 = \begin{cases} (a_{nano} - a_{barrier})/a_{barrier} & \text{inside the structure,} \\ 0 & \text{in the barrier.} \end{cases} \tag{3}$$

$$\alpha = \begin{cases} \frac{1}{2}C_{xxxx} + C_{xxyy} & \text{inside the structure,} \\ 0 & \text{in the barrier.} \end{cases} \tag{4}$$

The components of the strain tensor are computed directly from the three components of the displacement vector **u** which minimizes E_{CE}:

$$e_{ij}(\mathbf{r}) = \frac{1}{2}\left(\frac{\partial u_i(\mathbf{r})}{\partial r_j} + \frac{\partial u_j(\mathbf{r})}{\partial r_i}\right) \tag{5}$$

The components of the strain tensor are calculated directly from the displacement *u* that minimizes the action integral for the strain tensor.[1,2,28] The displacements are typically discretized at the nodes of the grid representing their first derivatives by finite differences. The first derivative is averaged over the eight permutations of forward and backward differences.[2,28] Details of numerical implementations can be found elsewhere.[1,2,4,28]

2.3 Valence Force Field:

In the the valence force field (VFF) model,[29,30] the strain energy is expressed as a sum of the potential energies located in atomic bonds. The total VFF strain energy is calculated as the sum of the local strain energies over all atoms:[2]

$$E_{VFF} = \sum_i E_{VFF}^{(i)} = \sum_{ij} V_2(\mathbf{R_i} - \mathbf{R_j}) + \sum_{ijk} V_3(\hat{\Theta}_{ijk}) + ... \tag{6}$$

where V_2 is a two-body term, and V_3 is a three-body function of the bond angle ($\hat{\Theta}_{ijk}$).

Taking only two- and three-body terms in Eq. (6), the VFF elastic energy is given by:

$$\begin{aligned} E_{VFF} &= \sum_{ij} V_2(\mathbf{R_i} - \mathbf{R_j}) + \sum_{ijk} V_3(\hat{\Theta}_{ijk}) = \sum_i \sum_j^{nn_i} \frac{3\alpha_{ij}^{(1)}}{8} \Delta d_{ij}^2 \\ &+ \sum_i \sum_{j,k>j}^{nn_i} \frac{3\beta_{jik}}{8 d_{ij}^0 d_{ik}^0} [(\mathbf{R_j} - \mathbf{R_i}) \cdot (\mathbf{R_k} - \mathbf{R_i}) - cos\theta_{jik}^0 d_{ij}^0 d_{ik}^0]^2 \end{aligned} \tag{7}$$

where $\Delta d_{ij}^2 = [((\mathbf{R_i} - \mathbf{R_j})^2 - (d_{ij}^0)^2)/d_{ij}^0]^2$, d_{ij}^0 is the ideal bond distance between the atoms i and j, θ_{jik}^0 is the ideal angle of the bond angle $j-i-k$. The $\sum^{nn_i}$ denotes summation over the nearest neighbors of atom i. The local-environment-dependent coefficients, $\alpha_{ij}^{(1)}$ and β_{jik}, bond-stretching and bond-bending distortions in bulk zinc-blende materials, respectively, are fitted to the elastic constants of bulk materials:

$$\begin{aligned} C_{11} + 2C_{12} &= \frac{\sqrt{3}}{4 d_{ij}} (3\alpha_{ij} + \beta_{ij}) \\ C_{11} - C_{12} &= \frac{\sqrt{3}}{4 d_{ij}} \beta_{ij} \\ C_{44} &= \frac{\sqrt{3}}{4 d_{ij}} \frac{4\alpha_{ij}\beta_{ij}}{\alpha_{ij}\beta_{ij}} \end{aligned} \tag{8}$$

These expressions do not account for Coulomb effects caused by the unequal charge distribution between the anion and cation sublattices in zinc-blende materials.[7] Neglecting the Coulomb correction causes slight deviation from the measured bulk properties.

The total strain energy including bond bending, bond stretching, and bond bending-bond stretching interactions is given by:[11]

$$\begin{aligned} E_{VFF} &= \sum_i \sum_j^{nn_i} \frac{3}{8} [\alpha_{ij}^{(1)} \Delta d_{ij}^2 + \alpha_{ij}^{(2)} \Delta d_{ij}^3] + \sum_i \sum_{j,k>j}^{nn_i} \frac{3\beta_{jik}}{8 d_{ij}^0 d_{ik}^0} [(\mathbf{R_j} - \mathbf{R_i}) \cdot (\mathbf{R_k} - \mathbf{R_i}) - cos\theta_{jik}^0 d_{ij}^0 d_{ik}^0]^2 \\ &+ \sum_i \sum_{j,k>j}^{nn_i} \frac{3\sigma_{jik}}{d_{ik}^0} \Delta d_{ij} [(\mathbf{R_j} - \mathbf{R_i}) \cdot (\mathbf{R_k} - \mathbf{R_i}) - cos\theta_{jik}^0 d_{ij}^0 d_{ik}^0] \end{aligned} \tag{9}$$

The second-order bond stretching coefficient $\alpha^{(2)}$ is related to the pressure derivative of the Young's modulus $d((C_{11} + 2C_{12})/3)/dP$.

The atomic positions $\{\mathbf{R}_i\}$ within the supercell are relaxed in order to determine the strain. The relaxed atomic configuration could be obtained, for example by conjugate gradient minimization of E_{VFF} with respect to the atomic positions.[2]

2.4 Discussion:

All discussed models are based on the elastic constants of the underlying bulk materials. However, the IE and CE models belong to continuum approaches, thus (i) they are not able to describe the strain at the level of the crystal unit cell, (ii) the large strains that exist between lattice-mismatched III-V semiconductors bring the CE outside the linearity regime,[2,11] and (iii) they "see" the geometrical symmetry rather than the real point group symmetry of the nanosystem.[2,37]

3 Single Particle States

As the next step in the modeling, the single particle states are calculated. We discuss the main features of commonly used single- and multi-band effective mass, tight binding, and empirical pseudopotential methods. They are parameterized by a set of experimentally obtained band structure parameters from the bulk material. If measurements on a nanostructure are performed in external electric or magnetic field, these external field effects enter the calculations at this step.

3.1 Effective-Mass Theory:

The effective-mass theory is a very well established method to obtain the band structure in the case of weak perturbing inhomogeneous semiconductor potentials.[38–42] Electron and hole energies near the band extrema in the presence of external magnetic and electric fields and in a crystal containing a shallow impurity were successfully described by this theory.[5,39,40,43]

The basic idea behind the effective mass theory is actually rather simple:[5] Near the band edges the electrons can be described to behave as if they are in free space except their masses taking some effective value m^*. The electron states are described by a single Schrödinger equation around the given point of the Brillouin zone, assuming the (conduction) band parabolic.* The physical accuracy of this simple effective mass approach decreases as one wanders away from the high symmetry points since the band non-parabolicity originating from band mixing, or inter-valley mixing, starts to be important.

In the framework of the effective-mass approach, this limitation was overcome by employing the model referred to as $\mathbf{k}\cdot\mathbf{p}$ theory.[39,40,43] It is based on selecting a few 3D-periodic Bloch orbitals taken from the Brillouin zone center which single particle wavefunctions are expanded in. The most studied is the structure description around the Γ point. In $\mathbf{k}\cdot\mathbf{p}$ theory, the coupling between the bands of interest (set A) and all other bands (set B) is reduced to zero whereas the coupling between the bands of interest was not affected by this transformation. At the same time the effective masses in the bands of interest are renormalized to take into account the influence of the bands in set B (Löwdin renormalization[44]). Next, a fitting procedure is used to obtain the effective-mass parameters.[43]

Depending on the analyzed system, the number of bands in the set A can vary from four up to thirty. Namely, 4×4 $\mathbf{k}\cdot\mathbf{p}$ model includes only heavy holes and light hole bands,† and is used when the energy gap and split-off energy are large enough so band mixing between heavy or light hole and the conduction band

* Strictly speaking such a picture is valid only at the high symmetry points of the Brillouin zone.
† Due to the spin, one ends up with four bands.

and split-off band can be neglected. For example, such a model has been employed to describe confined electron and hole energy levels in GaAs/(Al,Ga)As QDs with parabolic in-plane potential and step like potential in the growth direction.[45] Furthermore, to take into account the split-off band in materials with small split-off energy, basis set A was extended to include the split-off band, resulting in the 6×6 **k**·**p** model. In this case, it is assumed that the energy gap is large enough so the band mixing between valence band states and lowest laying conduction band can be neglected. For example, this model was used to investigate the electronic structure of InP/(In,Ga)P quantum dots and molecules.[46,47] In the case of materials with narrow band gap, e.g., InAs, the lowest lying conduction band has to be added to the set A, resulting in the 8×8 **k**·**p** model. Further extension of the basis set are possible, resulting in the 14×14,[48,49] or even 30×30 **k**·**p** models.[15,50] Clearly, adding more bands, extends the validity of a effective mass model further from the zone center, so that 30×30 **k**·**p** model gives the description of the whole Brillouin zone.[50] Going beyond 8×8 **k**·**p** model is necessary for indirect gap materials, such as AlAs, or Si. For example, Si/Ge QW and QDs have been successfully investigated in the framework of 30 band **k**·**p** theory.[15]

Derivation of the model for bulk – As we have already mentioned, a loosely bound outer shell electron in a semiconductor crystal can be best described by a particle traveling in a slowly varying periodic potential. The one electron Schrödinger equation is:[5]

$$(\frac{p^2}{2m_0}+V(\mathbf{r})+\widehat{H}_{so})\Psi_{\mathbf{k}}(\mathbf{r})=E_{\mathbf{k}}\Psi_{\mathbf{k}}(\mathbf{r})\ , \tag{10}$$

where the first, second, and third term on the left-hand side correspond to the kinetic energy of the electron, the periodic crystal potential, and spin-orbit interaction respectively. The spin-orbit interaction, $\widehat{H}_{so}$, is given by:

$$\widehat{H}_{so}=\frac{\hbar}{4m_0^2c^2}(\nabla V\times\mathbf{p})\cdot\sigma+\frac{\hbar}{4m_0^2c^2}(\nabla V\times\mathbf{k})\cdot\sigma\ , \tag{11}$$

where σ is the Pauli operator. The main contribution to the spin orbit interaction comes from the core region of the atom where ∇V and **p** are very large (the first term on right-hand side of Eq. 11), whereas the second term is usually neglected since **k** is at most 1/2 a reciprocal lattice vector and hence small compared to **p**.

The Bloch function is given by:

$$\Psi_{\mathbf{k}}(\mathbf{r})=exp(i\mathbf{kr})u_{n\mathbf{k}}(\mathbf{r})\ . \tag{12}$$

where $u_{n\mathbf{k}}(\mathbf{r})$ has the periodicity of V(**r**), **k** lies in the first Brillouin zone, and n is the band index.

Substituting Eq. (12) into Eq. (10) gives:[40]

$$[\frac{p^2}{2m_0}+V(\mathbf{r})+\frac{h^2k^2}{2m_0}+\frac{\hbar}{m_0}\mathbf{k}\cdot\mathbf{p}+\frac{\hbar}{4m_0^2c^2}(\nabla V\times\mathbf{p})\cdot\sigma]u_{n\mathbf{k}}(\mathbf{r})=E_n(\mathbf{k})u_{n\mathbf{k}}(\mathbf{r})\ , \tag{13}$$

This approach leads to the **k**·**p** approximation named after the 4th term appearing in the Hamiltonian of Eq. (13). For fixed value $\mathbf{k}=\mathbf{k}_0$, Eq. (13) has a complete set of eigenfunctions $u_{n\mathbf{k}_0}(\mathbf{r})$ which completely span the space of functions periodic in the real space Bravais lattice. This set of states is called **k**·**p** representation.[5,40]

We use Γ point ($\mathbf{k_0}=0$) as the basis for a **k**·**p** representation‡ and theoretically the entire zone can be covered. For example, 15 bands (30 including spin-orbit interaction) can give the description of the whole Brillouin zone.[50]

‡ Γ point is the most suitable to use as a basis, since it is also the point of highest symmetry in the zone.

One can write $u_{n\mathbf{k}}(\mathbf{r})$ in terms of $u_{n\mathbf{k}_0}(\mathbf{r})$:

$$u_{n\mathbf{k}}(\mathbf{r}) = \sum_{n'=1}^{N} c_{n'n} u_{n'\mathbf{k}_0}(\mathbf{r}) \ , \tag{14}$$

where N is the number of bands used in the expansion.

Substituting Eq. (14) into Eq. (13), then multiplying Eq. (13) on the left by $u_{n\mathbf{k}_0}$, and finally performing the integration over the unit cell gives the $\mathbf{k}_0 \cdot \mathbf{p}$ representation:

$$\sum_{n'}^{N} \{ [E_n(\mathbf{k}_0) + \frac{h^2(k^2 - k_0^2)}{2m_0}] \delta_{nn'} + \frac{\hbar}{m_0} (\mathbf{k} - \mathbf{k}_0) \cdot \langle u_{n\mathbf{k}_0} | \mathbf{p} | u_{n'\mathbf{k}_0} \rangle + \\ + \frac{\hbar}{4m_0^2 c^2} \langle u_{n\mathbf{k}_0} | (\nabla V \times \mathbf{p}) \cdot \sigma | u_{n'\mathbf{k}_0} \rangle \} c_{n'n} = E_n(\mathbf{k}) c_{nn} \ . \tag{15}$$

If we focus on the region of the conduction and valence band extrema where most carriers sit (around the Γ point). The topmost valence states and the lowest-lying conduction band are close together and well separated from all other band edges. This fact enables division of all states into two sets: set A containing the bands of interest (in our case, the lowest lying conduction band and three topmost valence states) and set B containing remaining bands that have non-negligible effect on the states in A. The interactions between A and B are removed, whereas interactions in A are perturbatively renormalized to account for the influence of the bands in set B.[5,44]

Let us first consider the case without the spin-orbit interaction. The valence band maximum is derived from atomic p functions, X, Y, Z, which remain degenerate under the tetrahedral point group of the zinc-blende lattice to give the representation Γ_{15}. The conduction band is derived from S functions which give the tetrahedral representation Γ_1. Therefore, Eq. (14) written in the matrix form for N=4, where the influence of all bands outside s,p subspace is included perturbatively, has the following form:

$$H_4 = \begin{pmatrix} D_e & Bk_yk_z + iPk_x & Bk_xk_z + iPk_y & Bk_xk_y + iPk_z \\ Bk_yk_z - iPk_x & D_{h_1} & -N'k_xk_y & -N'k_xk_z \\ Bk_xk_z - iPk_y & -N'k_xk_y & D_{h_2} & -N'k_yk_z \\ Bk_xk_y - iPk_z & -N'k_xk_z & -N'k_yk_z & D_{h_3} \end{pmatrix} , \tag{16}$$

Here, $D_e = E_c + A_c k^2$, $D_{h_1} = E_v - L'k_x^2 - M(k_y^2 + k_z^2)$, $D_{h_2} = E_v - L'k_y^2 - M(k_x^2 + k_z^2)$, $D_{h_3} = E_v - L'k_z^2 - M(k_x^2 + k_y^2)$, E_c denotes the energy of the conduction band minimum, and E_v is the energy of the valence band maximum. P is the Kane matrix element defined as $P = -i(\hbar/m)\langle S|p_x|X\rangle$ and B arises because of the inversion asymmetry of zinc-blende semiconductors. The number of independent parameters in Eq. (16) comes from the symmetry arguments.[39,41,42] The parameters P, E_c, E_v come from the direct interaction between s and p wavefunctions, whereas A_c, B, L′, M, N′ result from the second order interactions due to the Löwdin perturbation[44] involving the states outside s-p subspace. A_c is the electron effective mass renormalized to include influence of remote bands. B has a finite value in zinc-blende semiconductors, but parameter B is usually neglected.[26] In what follows we shall assume the inversion symmetry of the system (B=0). L′, M, N′ can be expressed in the terms of scaled[39] parameters γ_i, where i=1,2,3:

$$\begin{aligned} L' &= (\hbar^2/2m)(\gamma_1 + 4\gamma_2) \ , \\ M &= (\hbar^2/2m)(\gamma_1 - 2\gamma_2) \ , \\ N' &= (\hbar^2/2m)(6\gamma_3) \ , \end{aligned} \tag{17}$$

where m is the electron mass. Parameters γ_i were first introduced by Luttinger to represent the second order interactions involving the states outside p subspace.[39] In our case, in which the conduction band is treated together with the valence bands i.e. s-p subspace, the Luttinger parameters have to be scaled to remove perturbative interaction with the lowest lying conduction band. Scaled Luttinger parameters are connected to the valence-band Luttinger parameters by the relations:[43] $\gamma_1 = \gamma_1^L - E_P/3E_g$, $\gamma_2 = \gamma_2^L - E_P/6E_g$, $\gamma_3 = \gamma_3^L - E_P/6E_g$, where E_g is the fundamental band gap, and E_P is related to the Kane matrix element by $E_P = 2mP^2/\hbar^2$.

Luttinger parameters can be written in a manner which explicitly reveals the contribution of all other states of symmetry Γ_1, Γ_{15}, Γ_{12}, or Γ_{25}.[51] This states are compatible with the s, p, d, and f orbitals respectively. The contribution of Γ_{25} symmetry is neglected here.§ The Luttinger parameters can be written as:[51]

$$\begin{aligned} \gamma_1 &= -1 + 2\sigma + 4\pi + 4\delta \ , \\ \gamma_2 &= \sigma - \pi + 2\delta \ , \\ \gamma_3 &= \sigma + \pi - \delta \ , \end{aligned} \tag{18}$$

where σ, π, and δ are defined by:

$$\begin{aligned} \sigma &= (1/3m)\textstyle\sum_j^{\Gamma_1} |\langle X|p_x|u_j\rangle|^2/(E_j - E_v) - E_P/6E_g \ , \\ \pi &= (1/3m)\textstyle\sum_j^{\Gamma_{15}} |\langle X|p_y|u_j\rangle|^2/(E_j - E_v) \ , \\ \delta &= (1/6m)\textstyle\sum_j^{\Gamma_{12}} |\langle X|p_x|u_j\rangle|^2/(E_j - E_v) \ . \end{aligned} \tag{19}$$

m is the free electron mass, **p** is the momentum operator, and E_v is the valence band energy in the absence of spin orbit interaction. The sum is over the basis states u_j of all remote bands of a given symmetry. Note that from the sum that goes over basis states of the Γ_1 symmetry (σ term in Eq. (19)) the lowest-lying conduction band is subtracted (second term of right-hand side of expression for σ) since the interaction between the lowest-lying conduction band and three topmost valence bands is already explicitly treated in our model.¶

When the spin-orbit interaction is included, the same s-p subspace is used but also the spin degree of freedom is taken into account. As a consequence we have eight states instead of four. The spin-orbit interaction splits the Γ_{15} states forming irreducible representations Γ_8 and Γ_7. Namely, coupling of angular momentum with the spin gives two possible values of total angular momentum (j=3/2 and j=1/2). The four states $|3/2, j_z\rangle$ form the irreducible representation Γ_8, whereas two $|1/2, j_z\rangle$ form the irreducible representation Γ_7.

Spin-orbit interaction may be represented by the single parameter, Δ, which is the spin-orbit splitting of the p states:

$$\Delta = -3i\left(\frac{\hbar}{4m_o^2c^2}\right)\langle X|\nabla V \times \mathbf{p}|Z\rangle \ . \tag{20}$$

It is most convenient to work with eigenfunctions of the total angular momentum $|j, j_z\rangle$ which diagonalize spin-orbit interaction.‖ The explicit form of the eight-band model can be found elsewhere.[3,5]

§ Contribution of f orbitals to the valence electronic structure of semiconductors is insignificant, and therefore usually neglected.[51]
¶ The lowest-lying conduction band belongs to the set A.
‖ The proper linear combinations of p functions and spin functions are taken to diagonalize the spin orbit interaction.[38,39]

For completeness, let us add that if the crystal structure has inversion symmetry the bands are double degenerate with respect to spin (Kramers theorem). In the theoretical description of zinc-blende semiconductors, such as GaAs, InAs, AlAs etc. it is assumed that inversion symmetry is approximately satisfied due to the small difference in the constituent atoms.

Presence of weak perturbing inhomogeneous semiconductor potentials leads to the introduction of the envelope function.[38,39] It means that detailed wavefunction is split into slow varying (envelope part) $F_n(r)$ and the cell periodic and more oscillatory Bloch functions $u_{n\mathbf{k}}(\mathbf{r})$ satisfying the Schrödinger's equation with band-edge energies:

$$\Psi(\mathbf{r}) = F_n(\mathbf{r})u_{n\mathbf{k}}(\mathbf{r}) \ . \tag{21}$$

Application to Nanostructures – Due to its simplicity, easy implementation of the strain effects, effects of an applied magnetic field, or growth on high index surfaces, the multi-band effective theory has been widely accepted as a reasonably good theoretical tool for the electronic structure description of semiconductor nanostructures. It has been proven to give a remarkable good agreement with the experimental data when employed to nanostructures, ranging from quantum wells to QDs, or recently to quantum rings.

When applied to nanostructure, the effective-mass parameters present in the multi-band model become spatially dependent, commonly varying abruptly through the interface between the nanostructure and the surrounding barrier material. Application of the multi-band Hamiltonian to a nanostructure can be understood as an application of the multi-band Hamiltonian, as in the bulk case, for the nanostructure (one bulk material), and the second application for the barrier material (second bulk material). Boundary conditions are then applied to connect solutions from both sides of the interface. Also, it is assumed for all constituent materials to have the identical Γ point. In general, such a Hamiltonian does not have to be Hermitian, and its Hermiticity actually depends on the choice of the boundary conditions at the heterointerface of a nanostructure. Although clear from above, we stress here that the validity of the effective mass approximation is broken when applied to nanostructures, since the condition of the weak perturbing potential is violated at the heterointerface. Indeed, the arbitrariness in the choice of the boundary conditions, as well as an unjustified application of the effective mass theory to abruptly varying potentials (beyond the valid range of the model) are the main week points of this approach.

Several approaches for electronic structure calculations of semiconductor nanostructures were put forward, that can be divided into three groups: (i) First one is based on the matching of bulk solutions across an interface, as we mentioned above, and the generalization of the bulk equation to the case of spatially varying composition.[52] This approach has been widely accepted in the literature and no unexpected or nonphysical behavior of the calculated electronic spectra of any of the modeled nanostructures has been reported. The main weakness of this approach is the absence of the possibility to trace and estimate errors coming from the employed boundary conditions, since they were *ad hoc* introduced only taking care about the Hermiticity of the Hamiltonian;[3] (ii) Second approach is based on the development of the envelope function approach for nanostructures, with an intention to resolve both, the boundary condition problem as well as the validity of the effective-mass approach when applied to nanostructures.[53,54] Namely, the envelope function expansion with zone-center eigenfunctions was applied to an entire nanostructure** making the envelope functions unique and circumventing the boundary condition problem. The later is simply resolved by the fact that envelope functions are smooth and continuous everywhere for well behaved wavefunctions, even at the abrupt interface.†† From the practical point of view, the multiband Hamiltonian developed in the framework of Burt's approach differs from the one discussed under (i) in the additional terms arising

** The same $U_n(R)$ are used throughout even though there are regions where they are not eigenstates of the local Hamiltonian.
†† The limited range of wavevectors is used in their plane expansion

because of the abrupt variation of the effective-mass parameters at the interface of the heterostructure. Such a Hamiltonian was first developed by Foreman,[51] and this approach is usually referred to as Burt-Foreman approach. It is worth mentioning, that all simplicity of the conventional approach with respect to the modeling of strain in nanostructures, effects of an external fields, growth on high index surfaces is preserved in this approach as well. Strain effects are incorporated in an adiabatic manner, as discussed in previous section, where the part of the inhomogeneity effects on the bandstructure is accounted for through the terms coupling the conduction and valence bands;[55] and (iii) The third approach was proposed by Foreman[56] and is based on a new first-principle envelope-function theory that includes all non-zero, first-principle derived terms.[57,58] The envelope functions are formulated in terms of atoms rather than bulk compounds, whereas a traditional bulk-crystal description can be obtained from the atomistic formulation via linear transformation of variables.

3.2 Tight-Binding method:

In the tight-binding method (TBM) the electronic states are considered to be linear combinations of atomic (s,p,d,...) orbitals.[59] The Hamiltonian matrix elements between the atomic orbital states are introduced as free parameters to be determined by fitting the band gaps and band curvatures, i.e., effective masses at critical points in the Brillouin zone.[60] ‡‡ The basis functions do not need to be explicitly evaluated, as the only information required to find the electronic structure of the system is the Hamiltonian matrix elements. They are written in the parametrized form, and the whole system is described by a parametrization scheme.[61]

Derivation of the model for bulk – Let us denote an atomic orbital located on an atom at $\mathbf{R_i}$ as $\phi_{i,\alpha}(\mathbf{r}-\mathbf{R_i})$. The atomic orbitals on different atomic sites are not orthogonal to one another. The orthogonal set can be created from the original set of atomic orbitals preserving its symmetry properties, using the Löwding scheme:[62]

$$\psi_{i\alpha} = \sum_{i',\alpha'} S^{-1/2}_{i\alpha i'\alpha'} \phi_{i'\alpha'} \tag{22}$$

where S is the overlap matrix.

For periodic systems, such as crystals, the Bloch sum is used to obtain the electronic structure. Starting from the orthogonal set in Eq. (22), the Bloch sum is taken over all the periodic images of this orbital:[61]

$$N^{-1/2} \sum_{R_i} e^{i\mathbf{k}\cdot\mathbf{R_i}} \psi_{i\alpha}(\mathbf{r}-\mathbf{R_i}) \tag{23}$$

Next, the Hamiltonian matrix elements are evaluated as a function of $\mathbf{k}$ using the sums given in Eq. (23) as a set of basis functions:

$$H_{i\alpha j\beta} = N^{-1} \sum_{R_i,R_j} e^{i\mathbf{k}\cdot(\mathbf{R_j}-\mathbf{R_i})} \times \int \psi^*_{i\alpha}(\mathbf{r}-\mathbf{R_i}) H \psi_{j\beta}(\mathbf{r}-\mathbf{R_j}) d\mathbf{r} \tag{24}$$

One of the two sums in Eq. (24) can be canceled with the factor N^{-1}, giving the sum over the periodic images of the two atomic sites:

‡‡ Depending on the number of orbitals and nearest neighbors used to represent the states, the TBM requires for the overlap integrals to be determined in terms of the measured direct and indirect band gaps and/or effective masses in the bulk material.

$$H_{i\alpha j\beta} = \sum_{R_j} e^{i\mathbf{k}\cdot(\mathbf{R_j}-\mathbf{R_i})} \times \int \psi^*_{i\alpha}(\mathbf{r}-\mathbf{R_i}) H \psi_{j\beta}(\mathbf{r}-\mathbf{R_j}) d\mathbf{r} \tag{25}$$

We then apply the *two-center approximation*. In essence, the potential part of the Hamiltonian is replaced by the potential due to *only* the two atoms upon which the orbitals are located, neglecting all three-center integrals. This means that the integral in Eq. (25) depends only upon the form of the Löwdin functions, which have the same symmetry as the corresponding atomic orbitals, and the vector $(\mathbf{R_j}-\mathbf{R_i})$ between the atoms.

The eigenstates of the system are obtained by solving the characteristic equation:[61]

$$\hat{H}|\psi_i\rangle = E_i|\psi_i\rangle \tag{26}$$

where the eigenstates are given in an atomic-like basis set , $\{\psi_{i\alpha}\}$. Typically, only a small number of basis functions are used, corresponding to the atomic orbitals in the energy range of interest.

As already mentioned, (i) the basis functions do not need to be explicitly evaluated, as Hamiltonian matrix elements are sufficient to find the electronic structure of the system; and (ii) The integral in Eq. (25) is replaced with a parameter which depends only upon the internuclear distance $|\mathbf{R_i}-\mathbf{R_j}|$ and the symmetry of the orbitals involved.

The band energy of the crystal is evaluated by integrating the density of states, $n(E)$

$$E_{band} = \int^{E_f} E n(E) dE \tag{27}$$

where E_f is the Fermi level.

All other parts of the energy are typically described by a pairwise function:

$$E_{rep} = \sum_{i\neq j} U_{ij} \tag{28}$$

For detailed review on tight-binding modeling of materials see e.g., Goringe et al.[61]

Application to Nanostructures – Electronic structure calculation of a nanostructure quite often requires detailed modeling of the local environment on an atomic scale and introduces material considerations into the calculations. From the electronic structure point of view, the employed treatment depends on whether a nanostructure is strained or not.[7] The difference in the treatment of the two cases comes from the dependence of matrix elements of the Hamiltonian between two orbitals on the positions of atoms. In a strain free nanostructure (lattice matched), the atoms constitute a crystal with uniform unit cells, whereas in a lattice -mismatched structures, one can roughly discern "unit cells", but these cells vary in size, and atomic positions within them.[7]

As and example, we will show here case of lattice-matched quantum dots, where the wavefunction is represented as a general expansion in terms of localized atomic-like orbitals:[7]

$$|\psi\rangle = \frac{1}{\sqrt{N_1 N_2 N_3}} \sum_{n_1=1}^{N_1} \sum_{n_2=1}^{N_2} \sum_{n_3=1}^{N_3} \sum_{\alpha} \sum_{\mu} C^{(\alpha\mu)}_{n_1 n_2 n_3} |\alpha\mu; \mathbf{R_{n_1,n_2,n_3}} + \mathbf{v}_\mu\rangle \tag{29}$$

where α denotes the atomic-like orbitals centered on the μ atoms within each cell (n_1, n_2, n_3). The wavefunction is normalized over a volume consisting of N_i cells in the $\mathbf{a_i}$ (i=1,2,3) direction.

For the lattice-mismatched systems, problem is that the cells are no longer regularly placed and displacements depend on the specific cell and atom type. Also, the nearest neighbor parameters depend upon the relative atomic positions, which, in general, vary from cell to cell. Unfortunately, not only the tight-binding parameters change, but also the overlaps of the true atomic orbitals from which the Löwdin functions are constructed.[7]

3.3 Empirical Pseudopotential Method:

In the empirical pseudopotential method (EPM), the crystal potential is represented by a linear superposition of atomic potentials, which are modified to obtain good fits to the experimental direct and indirect band gaps and effective masses.

In solving the Schrödinger equation, the electrons are split into core and valence electrons. The core electrons are tightly bound and respond very little to the presence of neighboring atoms, whereas the valence electrons occupy the outer shells and are involved in the bonding of the atoms together. Only valence electrons are considered in pseudopotential methods, and the core electrons are treated as if they are frozen in an atomic-like configurations. Consequently, the valence electrons are considered to be moving in a weak one-electron potential. The justification is provided by the Phillips-Kleinman cancellation theorem.[63]

The pseudopotentials were initially constructed only to reproduce one-electron eigenvalues and to be as weak as possible. The more complex methods for the construction of pseudopotentials focus on making the valence pseudoorbital resemble as much as possible the valence orbital beyond some fiducial core radius r_i, which depends on the principal angular momentum quantum number l, and imposes other conditions, typically including smoothness in some form. Discussion about choice of pseudopotentials and their construction is beyond the scope of this work, and detailed analysis can be found elsewhere.[11,64]

Derivation of the model for bulk – The pseudopotential Hamiltonian for an electron in the crystal consists of a kinetic-energy term and a weak position-dependent potential $V(\mathbf{r})$:[65]

$$H = -\frac{\hbar^2}{2m}\nabla^2 + V(\mathbf{r}) \tag{30}$$

The potential $V(\mathbf{r})$ is a linear combination of atomic potentials $V_\alpha(\mathbf{r})$. Given that the crystal potential is periodic, the pseudopotential is also a periodic function and can be expanded in reciprocal lattice vectors $\mathbf{G}$.

$$V(\mathbf{r}) = \sum_G V_0(\mathbf{G}) e^{i\mathbf{G}\mathbf{r}} \tag{31}$$

where the expansion coefficient is given by

$$V_0(\mathbf{G}) = \frac{1}{\Omega}\int d^3r V_0(\mathbf{r}) e^{-i\mathbf{G}\mathbf{r}} \tag{32}$$

Ω being the volume of the unit cell.

Simplifying Eq. (32) to a diamond lattice, which has only one type of atoms, we can write the potential in real space as:

$$V_0(\mathbf{r}) = V_\alpha(\mathbf{r}+\tau) + V_\alpha(\mathbf{r}-\tau) \tag{33}$$

where two-atom basis is taken and centered at the origin $\mathbf{R} = 0$, and τ denotes atomic basis vectors.

In reciprocal space, the potential is given by:

$$V(\mathbf{r}) = \sum_{\mathbf{G}} V_G^{ff} S(\mathbf{G}) e^{i\mathbf{G}\mathbf{r}} \tag{34}$$

where $S(\mathbf{G})$ is a structure factor and V_G^{ff} is a pseudopotential form factor, treated as an adjustable parameter in EPM.

Starting from the wavefunction composed of a plane wave component and a cell periodic part $\psi_k(r) = e^{ikr}u_k(r) = e^{ikr}\sum_{G'} U(G')e^{iG'r}$, we obtain Schrödinger equation in a matrix form:

$$\sum_{G}[(\frac{\hbar(\mathbf{k}+\mathbf{G})^2}{2m} - E)U(\mathbf{G}) + \sum_{G'} V_G^{ff}(|\mathbf{G}-\mathbf{G}'|)U(\mathbf{G}')] = 0 \tag{35}$$

The expression in Eq. (35) is zero when each term in the sum is zero. This, rather simple derivation of the EPM, contains only local pseudopotentials, neglecting the spin-orbit interaction. This simplified local EPM gives reasonable good predictions for optical gaps, but fails when it comes to valence-band states.[66]

When spin-orbit interaction is included, Schrödinger equation is of the form:

$$(-\frac{\hbar^2\nabla^2}{2m} + V(\mathbf{r}) + H_{so})\Psi(\mathbf{r}) = E\Psi(\mathbf{r}) \tag{36}$$

where H_{so} is the spin-orbit interaction term given by:

$$H_{so} = \frac{\hbar}{4m^2c^2}[\frac{1}{r}\frac{\partial V}{\partial r}]\mathbf{L}\sigma \tag{37}$$

where $\mathbf{L}$ is the angular momentum and σ is the Pauli spin matrices.

In the presence of spin-orbit interaction, the crystal wavefunction is a (2×1) spinor which has the following form:

$$\Psi_{\mathbf{k}\sigma} = \psi_{\mathbf{k}} - \sum_t \langle|\Phi_t|\psi_{\mathbf{k}}\rangle\Phi_{t\sigma} \tag{38}$$

where $\sigma = \pm 1$

The secular equation takes the form:

$$|H_{m'\mathbf{k}\sigma';m\mathbf{k}\sigma} - E\delta_{m'\sigma';m\sigma}| = 0 \tag{39}$$

where the matrix elements is given by:

$$H_{n\mathbf{k}\sigma';m\mathbf{k}\sigma} = E^0_{m\mathbf{k}}\delta_{n\sigma';m\sigma} + \langle|Psi_{n\mathbf{k}'\sigma'}|H_{so}|\Psi_{m\mathbf{k}\sigma}\rangle \tag{40}$$

where n and m are row and column indexes, respectively.

Application to Nanostructures – EPM can be directly applied to nanostructures. Screened-strain-dependent atomic pseudopotential $v_\alpha(\mathbf{r};\mathrm{Tr}(\varepsilon))$ are placed on each site of atom of type α. They are fitted to bulk properties of constituent materials making nanostructure (e. g., InAs/GaAs self-assembled QD, InAs for QD and GaAs for barrier) including bulk band structures, experimental deformation potentials and effective masses and directly feel strain effects via hydrostatic component of the strain tensor [$\mathrm{Tr}(\varepsilon)$], if strain is present in the system.

The total pseudopotential of the system V(**r**) is constructed by superposing the nonlocal spin-orbit interaction, V_{so}, to this local screened pseudopotential, $v_\alpha(\mathbf{r};\mathrm{Tr}(\varepsilon))$, of all atoms:[9,10,19]

$$V(\mathbf{r}) = V_{so} + \sum_{i,\alpha} v_\alpha(\mathbf{r} - \mathbf{R}_{i,\alpha}; Tr(\varepsilon)). \tag{41}$$

The single-particle electron $\{e_0, e_1, e_2,...\}$ and hole $\{h_0, h_1, h_2,...\}$ states are extracted from the single-particle Schrödinger equation:[9,10]

$$\{-1/2\nabla^2 + V(\mathbf{r})\}\psi_i = E_i\psi_i \ , \tag{42}$$

Depending on the size of the system, two basis sets are employed.[9–11] For structures up to a few hundred thousand atoms, a plane wave basis set is used:[9,11]

$$\Psi_i = \sum_{\mathbf{G}} c_i(\mathbf{G}) e^{i\mathbf{G}\mathbf{r}} \tag{43}$$

where $c_i(\mathbf{G})$ are the expansion coefficients. The Hamiltonian matrix is large ($\sim$ several millions), but sparse. The kinetic energy term is calculated in Fourier space, where it is diagonal, and the potential energy part in real space.[9,11]

For large nanostructures, several million atoms, the basis set is constructed from a linear combination of strained bulk Bloch states, $\phi_{nk}(\mathbf{r},\varepsilon)$ from n bands, k k-points, and taken at a few strain values ε:[10,11]

$$\Psi_i(\mathbf{r},\varepsilon) = \sum_{n,k} c_{n,k}^{(i)} \phi_{nk}(\mathbf{r},\varepsilon) \tag{44}$$

The Hamiltonian matrix is small ($\sim$ few tens of thousands) with this basis set. Whole matrix can be easily stored in the memory, and it is diagonalized for several eigenvalues.[10,11]

For further reading on pseudopotential methods in condensed matter applications we recommend Pickett,[64] and on EPM in materials and nanostructures recent review by Bester.[11]

3.4 Implementation of Effects of an External Magnetic Field to Nanostructures

From the theoretical point of view, the effects of an external electric field are included through Peierls substitution in the wave-vector and by the Zeeman energy term. However, complications can arrise in the numerical implementation. These comlications are typically related to the choice of the gauge and breaking of the gauge invariance. In what follows, we will briefly discuss how magnetic field should be implemented theoretically and what are the known issues in the implementation in the effective-mass, tight-binding, and pseudopotential methods.

Magnetic field **B** is defined via magnetic vector potential **A**:

$$\mathbf{B} = \nabla \times \mathbf{A} \ . \tag{45}$$

A is not unique, so if **A** is the vector potential for **B**, then so is $\mathbf{A} + \nabla\chi$, where χ is an arbitrary scalar function. This nonuniqueness leads to a degree of freedom(gauge freedom) and requires choosing a gauge.

In a gauge transformation, the vector potential transforms as $\mathbf{A} \to \mathbf{A} + \nabla\chi$, and state $\psi(\mathbf{r} \to G(\mathbf{r})\psi(\mathbf{r})$, where $G(\mathbf{r}) = exp(-i(e/\hbar)\chi(\mathbf{r}))$. If the theory is gauge invariant, then all physical quantities must be independent of such transformations. For example, if $\chi = \chi(y,z)$, then $\langle x\rangle \to \langle G^+xG\rangle$, where $G^+xG \neq x$. No theory can be gauge invariant if x, y, z do not commute.

From a purely practical point of view, this can be interpreted as follows. If a model nanostructure defined in a supercell/computational box is exposed to an external **homogeneous** magnetic field, then single particle energy levels and wavefunctions should not be sensitive to the choice of the gauge and/or the position of nanustructure within the cell/box. This lead to the two basic tests that *each and every correct implementation* of an homogeneous magnetic field should satisfy within the numerical accuracy. The single particle energy levels and wavefunctions (i) should not be influenced by changing the gauge, e.g., going from Landaue to Symmetric gauge; (ii) should not be be affected by the position of the nanostructure within the cell/box.

Implementation in the effective mass $\mathbf{k}\cdot\mathbf{p}$ *method:* Theoretically, the effects of a magnetic field in an effective mass Hamiltonian are included through Peierls substitution in the wave-vector and by adding the Zeeman energy term.[38,39] This Hamiltonian is gauge invariant. However, "numerically implemented" Hamiltonian, e.g., discretized on the grid, has to mantain all the properties of the continuum one for a gauge transformation of the vector potential. If this condition is not fulfilled large errors in the estimates of eigenvalues and corresponding eigenvectors may occur. To illustrate *correct* gauge invariant implementation, we consider Hamiltonian with Peierls substitution for the wave vector, discretized on a grid. We use Wilson's formulation of the lattice gauge theory.[4,5,67] We impose the condition that a discretized Hamiltonian maintains all its physical properties if a gauge transformation of the vector potential has been performed.[4,5,67]

If the vector potential transforms as $\mathbf{A}\rightarrow\mathbf{A}+\nabla\chi$, then a wave function representing a pysical state of the system transforms as $\Psi(\mathbf{r})\rightarrow G(\mathbf{r})\Psi(\mathbf{r})$, where $G(\mathbf{r})=exp(-i(e/\hbar)\chi(\mathbf{r}))$, e - electron charge, $\hbar$ - Planck constant. As a consequence, the Hamiltonian transforms as $H\rightarrow G(\mathbf{r})HG^{+}(\mathbf{r})$.

Considering an uniform discretization grid, the lattice operator $U_j(\xi)$, can be defined as:

$$U_j(\xi)=exp(-i(e/\hbar)a_{latt}A_j(\xi))\ , \tag{46}$$

where j=x,y,z, a_{latt} - is the grid spacing, and $\xi=(la_{latt},ma_{latt},na_{latt})$ defines the position on the grid. $U_j(\xi)$ can be understood as the link variable between two points on the grid, and it transforms as:[4,68]

$$U_j(\xi)\rightarrow G^{+}(\xi)U_j(\xi)G(\xi+j) \tag{47}$$

Using previous expressions, one obtains correct discretization scheme. For example, the discretization of the second derivative is given by:[4,68]

$$\frac{\partial^2\psi}{\partial x^2}\rightarrow\frac{U_x^{+}(i,j,k)\psi_{i+1,j,k}-2\psi_{i,j,k}+U_x(i+1,j,k)\psi_{i-1,j,k}}{a_{latt}^2}\ . \tag{48}$$

Using the discretization scheme illustrated by Eq. (48), the phase of the wave functions gets preserved. It is important to stress that the phase should be preserved at the edges of the computational box by using the correct choice of the boundary conditions. For example, imposing Dirichlet boundary conditions ensures phase preserving of the wave functions.

Implementation in the tight-binding method: Tight-binding Hamiltonians are often used to discretize the Schr"odinger equation on a lattice. In order to include external magnetic field into the model, effects of discretization on the gauge invariance should be considered.

The simplest proposed solution is given by:[68,69]

$$H_{TB}=\sum_x[N_d(\hbar^2/ma_{latt}^2)+V(bfr)]|x\rangle\langle x|+\sum_x\sum_{y\neq x}(-\frac{\hbar^2}{2ma^2})exp(i\theta_{x,y})|x\rangle\langle y| \tag{49}$$

This approach is based on a cubic lattice, and sifficient accuracy can be achieved only with an extremly large basis. There are a few other apporaches in the framework of tight-binding approach to preserve the gauge invariance, but they cannot descirbe intra-atomic transitions.[69] Foreman proposed a tight-binding model that can be made a gauge invarinat where the basis can be constructed from the symmetrized coordinate eigenkets.[69]

Implementation in the empirical pseudopotential method: The psedopotential Hamiltonian in the presence of a magnetic field should behave in the same way as the all-electron Hamiltonian. The effects of a magnetic field are included through Peierls substitution in the wave-vector and by adding the Zeeman energy term. The main issue is how to deal with non-local potential:[70,71]

$$V_{nl}(\mathbf{r}, bfr') = \langle \mathbf{r}|V_{nl}|\mathbf{r}'\rangle \neq 0, for\ \mathbf{r} \neq \mathbf{r}'. \quad (50)$$

Given Eq. (50), the gauge invariance demands that V_{nl} depends on the vector potential $\mathbf{A}$: $\langle \mathbf{r}|V_{nl}|\mathbf{r}'\rangle = V_{nl} exp(-ie/\hbar c) \int \mathbf{A} d\mathbf{r}$.[70,71]

3.5 Discussion:

The simplest, single-band effective mass method, has been widely used to predict basic optical properties of nanostructures. Although, decoupling of bands, as done in the single-band model, introduces significant errors in energy prediction, a 3D application that includes realistic QDs' geometry is often accepted as a good first approximation, especially by the experimentalists. Implementation of a multi-band model appears as a reasonable compromise between the simplicity and inclusion of most relevant effects present in semiconductor nanostructures, where maybe the most studied are III-V semiconductor QDs. Advantages of this approach are easy treatment of strain effects, external electric and magnetic field, growth on high index surfaces. Main drawbacks of the multi-band effective mass model are limited number of bands used in expansion (not all relevant band mixing may not be included), omission of atomistic symmetry (only geometric one is present).[5] Tight-binding and EPM are certainly more accurate and capture atomistic effects. They have been successfully applied to describe optical properties of various nanostructures. It has been argued that the tight-binding models lack atomistic wavefunctions, because of direct parametrization of the Hamiltonian.[11]

All the methods we analyzed here are empirical, and their parameters' sets are typically fitted to experimental data. The lack of the accuracy of the input parameters, limits the predictions of these methods. However, the *ab initio* methods, such as Hartree-Fock, Density Functional Theory, or GW, which calculate electronic structure from first principles, can not be used because of the size of nanostructures. The *ab initio* methods have been used to calculate up to a few hundred atoms (<500 atoms), whereas a typical nanostructure contains few hundred thousands of atoms. The importance of *ab initio* methods comes from the need to improve accuracy of input parameters and/or to be used as benchmark.

4 Exciton Complexes in Nanostructures

Presence of N_h holes and N_e electrons in a nanostructure creates exciton complexes; neutral excitons, if $N_h = N_e$, or charged excitons if $N_h \neq N_e$. Coulomb interaction, including exchange and correlation effects between carriers in a nanostructure reveals an interesting playground for investigation of many particle physics in confined spaces.[19,72] The fingerprints of exciton complexes are best seen in the emission spectra, where spectroscopic transitions result from the recombination of an electron in the conduction band with

a hole in the valence band, where N_e-1 and N_h-1 spectator electrons and holes, respectively, occupy other electronic levels. In that respect, the spectroscopy of self-assembled semiconductor QDs is quite remarkable, revealing an amazingly rich set of very sharp excitonic lines in a single-dot emission spectrum.[20,73–75] This not the case with colloidal nanocrystals where efficient non-radiative Auger recombination of exciton complexes prevents radiative emission.[72,76]

In the emission spectra of individual self-assembled semiconductor QDs, various exciton complexes have been identified unambiguously either by tuning the excitation intensity[24] or direction and amplitude of an electric field in which the QD is embedded.[74,75] There have been various theoretical studies of exciton complexes, with different levels of complexity. The simplest approach is perturbation theory approach, based on the simple counting of interactions between carriers, often disregarding the morphology of the QD.[77] The more complex theoretical models, take into account QD morphology (e.g., by assuming QD size, shape, and composition), strain effects and piezo effects, predicting emission spectra.[19,21,72–74] The nature of many-particle interaction, such as electron-hole Coulomb effects, electron-hole exchange interaction, or correlations can be extracted from configuration-interaction (CI) method.

4.1 Configuration Interaction Method:

Exciton complexes are calculated using the configuration interaction (CI) method,[19,26,72,78–80] taking into account direct Coulomb interaction, exchange and correlation effects.

The many-body state is expanded into configurations built from the ground and excited single particle states. Antisymmetrized products of single particle wavefunctions accounting for direct Coulomb interaction and exchange, whereas the correlation effects are accounted for by expanding the basis to include excited-state-configurations.[73]

Slater determinants $\Phi_{v,c}$ are constructed from single-particle electron and hole orbitals. The multiexciton wavefunctions Ψ are expanded in terms of this determinal basis set:[19,78]

$$\Psi = \sum_{v=1}^{N_v} \sum_{c=1}^{Nc} C_{v,c}^{\alpha} \Phi_{v,c} \ , \tag{51}$$

where N_v and N_c denote the number of valence and conduction states included in the expansion of the multiexciton wavefunction. In the notation the valence states are numbered from 1 to N_v in order of decreasing energy starting from the valence-band maximum, while the conduction states are numbered from 1 to N_c in order of increasing energy starting from the conduction-band minimum.

The matrix elements of the many-particle Hamiltonian H in the basis set $\{\Psi_{v,c}\}$ are calculated as

$$H_{v,c,v',c'} = \langle \Phi_{v,c} | H | \Phi_{v',c'} \rangle = (E_c - E_v)\delta_{v,v'}\delta_{c,c'} - J_{vc,v'c'} + K_{vc,v'c'} \ , \tag{52}$$

where J and K are the Coulomb and exchange integrals, respectively:

$$J_{vc,v'c'} = e^2 \sum_{\sigma_1,\sigma_2} \int\int \frac{\psi_{v'}^*(\mathbf{r}_1,\sigma_1)\psi_c^*(\mathbf{r}_2,\sigma_2)\psi_v(\mathbf{r}_1,\sigma_1)\psi_{c'}(\mathbf{r}_2,\sigma_2)}{\overline{\varepsilon}(\mathbf{r}_1,\mathbf{r}_2)|\mathbf{r}_1,\mathbf{r}_2|} d\mathbf{r}_1 d\mathbf{r}_2 \ , \tag{53}$$

$$K_{vc,v'c'} = e^2 \sum_{\sigma_1,\sigma_2} \int\int \frac{\psi_{v'}^*(\mathbf{r}_1,\sigma_1)\psi_c^*(\mathbf{r}_2,\sigma_2)\psi_{c'}(\mathbf{r}_1,\sigma_1)\psi_v(\mathbf{r}_2,\sigma_2)}{\overline{\varepsilon}(\mathbf{r}_1,\mathbf{r}_2)|\mathbf{r}_1,\mathbf{r}_2|} d\mathbf{r}_1 d\mathbf{r}_2 \ , \tag{54}$$

Coulomb and exchange integrals (Eqs. 53 and 54) are computed numerically from the pseudopotential single-particle orbitals. The screening function for these integrals $\overline{\varepsilon}(\mathbf{r}_1,\mathbf{r}_2)$ contains an ionic and an

electronic component that exhibit a smooth transition from unscreened at short range to screened at long range.[11,78]

5 Post-Processors

Postprocessor tools are various and include calculation of the multiexcitonic emission spectra,[19–21] fine structure splittings of exciton complexes, energy transfer for semiconductor nanocrystals,[23] charging energies, entanglement[6,24] to name just a few.

5.1 Optical Properties of Nanostructures

The emission intensity spectrum of a (multi)exciton, χ, for polarization vector $\hat{\mathbf{e}}$ of the electromagnetic field, is given by:[81]

$$I^{(\mathbf{e})}(\omega,T,\chi)=\sum_{i,f}|M_{if}^{(\mathbf{e})}(\chi)|^2P_i(T,\chi)\delta[\omega-\omega_{if}(\chi)] \tag{55}$$

where

$$M_{if}^{(\mathbf{e})}(\chi)=\langle\Psi^{(f)}(\chi-1)|\hat{\mathbf{e}}\cdot\mathbf{p}|\Psi^{(i)}(\chi)\rangle\ , \tag{56}$$

$$P_i(T,\chi)=Nexp[-\frac{E^{(i)}(\chi)-E^{(0)}(\chi)}{k_BT}]\ , \tag{57}$$

are the transition dipole matrix element and occupation (Boltzmann) probability of the initial state at temperature T, respectively. The transition energy is $\omega_{if}(\chi)$.

In the case of semiconductor III-V self-assembled QDs, such as (In,Ga)As/GaAs QDs, there is a strong anisotropy between the [001] and [xy0] polarization directions, and weaker anisotropy between [110] and $[1\bar{1}0]$.[26] The polarization anisotropy between the [110] and $[1\bar{1}0]$ directions:

$$p=\frac{I_{1\bar{1}0}-I_{110}}{I_{1\bar{1}0}+I_{110}}\ . \tag{58}$$

Eq. (58) reflects the C_{2v} symmetry of the single-particle wavefunctions. This quantity is particularly important for the emission from mono-exciton (X^0) in a $Ga_{1-x}In_xAs$/GaAs QD. The fine-structure splitting (FSS) of X^0 yields two optically active transitions split typically by a few tens of μeV, and each linearly polarized along two orthogonal axes of the QD.[73] The magnitude of the FSS and the polarization directions of two transitions have attracted recently special attention because of potential application of QD's as single photon sources.[82] The requirement for a QD in such applications is that the emitted photons would be distinguishable only by polarization so the FSS needs to vanish.

5.2 Electronic Energy Transfer

The electronic energy transfer (EET) is defined as a transfer of the excitation energy from an electronically excited donor system, such as atom, or nanocrystal, to a nearby acceptor, in a nonradiative way.[23,83] For example, EET was demonstrated between QDs, organic polymers and QDs, etc.

The rate of EET between a single electronic state of a donor and acceptor is given by:[23,83]

$$k = \frac{2\pi}{\hbar}|sV_s|^2 J \tag{59}$$

where V_s is the electronic coupling between donor and acceptor transition densities, s is the solvent screening factor, and J is the normalized overlap between donor emission and acceptor absorption spectra.

The electronic coupling, V_s can be calculated as:

$$V_s^{(3D)} = \int \frac{\rho_{g,e}^D \rho_{e,g}^A}{\mathbf{r}_1 - \mathbf{r}_1} d\mathbf{r}_1 d\mathbf{r}_2 \ , \tag{60}$$

where $\rho_{g,e}^D$ and $\rho_{e,g}^A$ are transition densities, and, for the case of QD-QD EET, given by

$$\rho_{e,g} = \sum_{\sigma} \psi_v^*(\mathbf{r},\sigma)\psi_c(\mathbf{r},\sigma) \tag{61}$$

where $\psi_c($**r** and $\psi_v($**r** are single-particle conduction and valence wavefunctions, respectively.

The electronic coupling, V_s, given by Eq. (60), is Coulombic and represents coupling between transition densities connecting the ground state and excited state for the donor and acceptor. V_s can be calculated directly from Eq. (60). However, quite often the point-dipole approximation, coming from Förster theory, gets employed, where the electronic coupling, expanded as multipole series, is obtained by truncating the expansion to the interaction between transition dipole moments:[23,84]

$$V_s \approx= V_{dip-dip} = \frac{\kappa \mu_D^T \mu_A^T}{R^3} \ , \tag{62}$$

where κ is the orientation factor, given in the terms of the angles between transition moments and donor-acceptor vector, and $\mu_i^T, i = D,A$ are transition dipole moments of D and A separated by a distance R. In the case of QDs they are defined:

$$\mu^{QD} = \int r_\alpha \rho_{eg}^{QD}(\mathbf{r}) d\mathbf{r} \tag{63}$$

where $\alpha = x,y,z$

Transition densities can be obtained from single particle wavefunctions, using methods described in Sec. 3. For example, analysis of EET involving QD-QD pairs was performed using empirical tight-binding[84] and empirical pseudoptential methods.[23]

The validity of approximation for EEC given by Eq. (62), leads to the Förster resonance energy transfer (FRET). FRET is an important communication and transport mechanism on the nanoscale, thus the interest in controling this process in assemblies of QDs, or on the single donor-acceptor pair level.[84,85] FRET between QDs has been already investigated in closely packed mixed layers and separated donor and acceptor layers.[85–87]

5.3 Charging Energies

The charging energy is the energy required to add one more carrier to a nanostructure already charged with N-1 carriers: $\mu(N) = E(N) - E(N-1)$.[88] E(N) are ground state energy of N-particle nanostructure.

References

1 M. Grundmann, J. Christen, N. N. Ledentsov, J. Böhrer, D. Bimberg, S. S. Ruvimov, P. Werner, U. Richter, U. Gösele, J. Heydenreich, V. Ustinov, A. Y. Egorov, A. E. Zhukov, P. S. Kopev and Z. I. Alferov, *Phys. Rev. Lett.*, 1995, **74**, 4043.
2 C. Pryor, J. Kim, L. W. Wang, A. J. Williamson and A. Zunger, *J. Appl. Phys.*, 1998, **83**, 2548.
3 V. Mlinar, M. Tadic, B. Partoens and F. M. Peeters, *Phys. Rev. B*, 2005, **71**, 205305.
4 V. Mlinar and F. M. Peeters, *J. Mater. Chem.*, 2007, **17**, 3687.
5 V. Mlinar, *PhD thesis*, Department of Physics, University of Antwerp, 2007.
6 G. Bester and A. Zunger, *Phys. Rev. B*, 2005, **72**, 165334.
7 G. Klimeck, F. Oyafuso, T. B. Boykin, R. C. Bowen and P. von Allmen, *CMES-computer modeling in engineering and sciences*, 2002, **3**, 601.
8 G. Bryant, *Phys. Rev. B*, 1993, **48**, 8024.
9 L.-W. Wang and A. Zunger, *J. Phys. Chem.*, 1994, **98**, 2158.
10 L. W. Wang and A. Zunger, *Phys. Rev. B*, 1999, **59**, 15806.
11 G. Bester, *J. Phys.: Condens. Matter*, 2009, **21**, 023202.
12 V. Mlinar and A. Zunger, *Phys. Rev. B*, 2009, **79**, 115416.
13 O. Stier, M. Grundmann and D. Bimberg, *Phys. Rev. B*, 1999, **59**, 5688.
14 C. Pryor, *Phys. Rev. B*, 1999, **60**, 2869.
15 M. E. Kurdi, S. Sauvage, G. Fishman and P. Boucaud, *Phys. Rev. B*, 2006, **73**, 195327.
16 S. Tomić, A. G. Sunderland and I. J. Bush, *J. Mater. Chem.*, 2006, **16**, 1963.
17 N. Vukmirovic, D. Indjin, V. Jovanovic, Z. Ikonic and P. Harrison, *Phys. Rev. B*, 2005, **72**, 75356.
18 N. Vukmirovic, Z. Ikonic, I. Savic, D. Indjin and P. Harrison, *J. Appl. Phys.*, 2006, **100**, 74502.
19 V. Mlinar and A. Zunger, *Phys. Rev. B*, 2009, **80**, 205311.
20 V. Mlinar and A. Zunger, *Phys. Rev. B*, 2009, **80**, 035328.
21 A. Schliwa, M. Winkelnkemper and D. Bimberg, *Phys. Rev. B*, 2009, **79**, 075443.
22 A. Schliwa, M. Winkelnkemper, A. Lochmann, E. Stock and D. Bimberg, *Phys. Rev. B*, 2009, **80**, 161307.
23 C. Curutchet, A. Franceschetti, A. Zunger and G. D. Scholes, *J. Phys. Chem. C*, 2008, **112**, 13336.
24 M. Bayer, P. Hawrylak, K. Hinzer, S. Fafard, M. Korkusinski, Z. R. Wasilewski, O. Stern and A. Forchel, *Science*, 2001, **291**, 451.
25 M. Grundmann, O. Stier and D. Bimberg, *Phys. Rev. B*, 1995, **52**, 11969.
26 O. Stier, *PhD thesis*, Technische Universität Berlin, 2001.
27 J. H. Davies, *J. Appl. Phys.*, 1998, **84**, 1358.
28 B. Jogai, *J. Appl. Phys.*, 2000, **88**, 5050.
29 P. N. Keating, *Phys. Rev.*, 1966, **145**, 637.
30 R. M. Martin, *Phys. Rev. B*, 1970, **1**, 4005.
31 V. Mlinar and F. M. Peeters, *Appl. Phys. Lett.*, 2007, **91**, 021910.
32 W. Neumann, H. Kirmse, I. Häusler and R. Otto, *Journal of Microscopy*, 2006, **223**, 200.
33 K. Tillmann, M. Lentzen and R. Rosenfeld, *Inst. Phys. Conf. Ser.*, 1999, **164**, 15.
34 P. L. Galindo, A. Yánez, J. Pizarro, E. Guerrero, T. Ben and S. I. Molina, proceedings (Congress XIV Microscopy of Semiconducting Materials, Oxford, 2005-04-11 to 2005-04-14).
35 E. Guerrero, P. Galindo, A. Yánez, T. Ben and S. I. Molina, Microscopy and Microanalysis.
36 J. D. Eshelby, *Proc. R. Soc. London, Ser. A*, 1957, **241**, 376.
37 G. Bester and A. Zunger, *Phys. Rev. B*, 2005, **71**, 45318.
38 J. Luttinger and W. Kohn, *Phys. Rev.*, 1955, **97**, 869.
39 J. Luttinger, *Phys. Rev.*, 1956, **102**, 1030.
40 E. O. Kane, *J. Phys. Chem. Solids*, 1957, **1**, 249–261.
41 M. Weiler, R. Aggarwal and B. Lax, *Phys. Rev. B.*, 1978, **17**, 3269.
42 M. H. Weiler, *Semiconductors and Semimetals*, Academic Press, New York, 1981, ch. 3, pp. 119–191.
43 C. Pidgeon and R. Brown, *Phys. Rev.*, 1966, **146**, 575.
44 P. Löwdin, *J. Chem. Phys.*, 1951, **19**, 1396.
45 F. B. Pedersen and Y. C. Chang, *Phys. Rev. B*, 1996, **53**, 1507.
46 M. Tadić, F. M. Peeters and K. L. Janssens, *Phys. Rev. B*, 2002, **65**, 165333.
47 V. Mlinar, M. Tadić and F. M. Peeters, *Phys. Rev. B*, 2006, **73**, 235336.
48 P. Pfeffer and W. Zawadzki, *Phys. Rev. B*, 1990, **41**, 1561.
49 M. E. Kurdi, G. Fishman, S. Sauvage and P. Boucaud, *Phys. Rev. B*, 2003, **68**, 165333.
50 S. Richard, F. Aniel and G. Fishman, *Phys. Rev. B*, 2005, **72**, 245316.
51 B. A. Foreman, *Phys. Rev. B*, 1993, **48**, 4964.
52 R. Eppenga, M. Schuurmans and S. Colak, *Phys. Rev. B*, 1987, **36**, 1554.
53 M. G. Burt, *J. Phys.: Condens. Matter.*, 1992, **4**, 6651.
54 M. G. Burt, *J. Phys.: Condens. Matter.*, 1999, **11**, 53.
55 Y. Zhang, *Phys. Rev. B*, 1994, **49**, 14352.
56 B. A. Foreman, *Phys. Rev. B*, 2005, **72**, 165345.

57 B. A. Foreman, *J. Phys.: Condens. Matter*, 2006, **18**, 1335.
58 B. A. Foreman, cond-mat/0701396.
59 J. T. Slater and G. F. Koster, *Phys. Rev.*, 1954, **94**, 1498.
60 D. J. Chadi and M. L. Cohen, *Phys. Status Solidi B*, 1974, **62**, 235.
61 C. M. Goringe, D. R. Bowler and E. Hernández, *Rep. Prog. Phys.*, 1997, **60**, 1447.
62 P. Löwdin, *J. Chem. Phys.*, 1950, **18**, 365.
63 J. C. Phillips and L. Kleinman, *Phys. Rev.*, 1959, **116**, 287.
64 W. E. Pickett, *Comp. Phys. Rep.*, 1989, 115.
65 M. L. Cohen and T. K. Bergstresser, *Phys. Rev.*, 1966, **141**, 789.
66 S. González, *MSc thesis*, Arizona State University, 2001.
67 K. Wilson, *Phys. Rev. D*, 1974, **10**, 2445.
68 M. Governale and C. Ungavelli, *Phys. Rev. B*, 1998, **58**, 7816.
69 B. A. Foreman, *Phys. Rev. B*, 2002, **66**, 165212.
70 S. Ismail-Beigi, E. K. Chang and S. G. Louie, *Phys. Rev. Lett.*, 2001, **87**, 87402.
71 C. J. Pickard and F. Mauri, *Phys. Rev. Lett.*, 2003, **91**, 196401.
72 V. Mlinar, A. Franceschetti and A. Zunger, *Phys. Rev. B*, 2009, **79**, 121307(R).
73 S. Rodt, A. Schliwa, K. Pötschke, F. Guffarth and D. Bimberg, *Phys. Rev. B*, 2005, **71**, 155325.
74 M. Ediger, G. Bester, A. Badolato, P. M. Petroff, K. Karrai, A. Zunger and R. J. Warburton, *Nature Physics*, 2007, **3**, 774.
75 E. Poem, J. Shemesh, I. Marderfeld, D. Galushko, N. Akopian, D. Gershoni, B. D. Gerardot, A. Badolato and P. M. Petroff, *Phys. Rev. B*, 2007, **91**, 235304.
76 V. I. Klimov, *Annu. Rev. Phys. Chem.*, 2007, **58**, 635.
77 M. Bayer, O. Stern, P. Hawrylak, S. Fafard and A. Forchel, *Nature*, 2000, **405**, 923.
78 A. Franceschetti, H. Fu, L. W. Wang and A. Zunger, *Phys. Rev. B*, 1999, **60**, 1819.
79 J. Shumway, A. Franceschetti and A. Zunger, *Phys. Rev. B*, 2001, **63**, 155316.
80 M. Rontani, C. Cavazzoni, D. Bellucci and G. Goldoni, *J. Chem. Phys.*, 2006, **124**, 124102.
81 G. A. Narvaez, G. Bester and A. Zunger, *Phys. Rev. B*, 2005, **72**, 245318.
82 M. Pelton, C. Santori, J. Vuckovic, B. Zhang, G. S. Solomon, J. Plant and Y. Yamamoto, *Phys. Rev. Lett.*, 2002, **89**, 233602.
83 G. D. Scholes, *Annu. Rev. Phys. Chem.*, 2003, **54**, 57.
84 G. Allan and C. Delerue, *Phys. Rev. B*, 2007, **75**, 195311.
85 V. K. Komarala, A. L. Bradley, Y. P. Rakovich, S. J. Byrne, Y. K. Gun'ko and A. L. Rogach, Proc. of SPIE, 2007, p. 66410Y.
86 C. R. Kagan, C. B. Murray, M. Nirmal and M. G. Bawendi, *Phys. Rev. Lett.*, 1996, **76**, 1517.
87 T. Franzi, D. Koktysh, T. A. Klar, A. L. Rogach, J. Feldmann and N. Gaponik, *Appl. Phys. Lett.*, 2004, **84**, 2904.
88 L. He, G. Bester and A. Zunger, *Phys. Rev. Lett.*, 2005, **95**, 246804.